Scientia Iranica A (2019) 26(4), 2258–2275

SCIENTIA IRANICA

Sharif University of Technology
Scientia Iranica
Transactions A: Civil Engineering
http://scientiairanica.sharif.edu

Invited Paper

A new higher-order strain-based plane element

M. Rezaiee-Pajand*, **N. Gharaei-Moghaddam, and MR. Ramezani**

School of Engineering, Ferdowsi University of Mashhad, Mashhad, Iran.

Received 3 March 2019; received in revised form 26 April 2019; accepted 20 May 2019

KEYWORDS
Strain-based formulation;
Second-order strain field;
Equilibrium condition;
Numerical evaluation;
Drilling degrees of freedom.

Abstract. This study proposes a new higher-order triangular plane element with drilling degrees of freedom by considering second-order strain field. In addition to the inclusion of drilling degrees of freedom and utilization of higher-order assumes strains, the satisfaction of equilibrium equations improves the performance of the suggested element in comparison to many of the other available elements. Following the proposition of the new element, a series of benchmark problems are solved to evaluate the performance of the suggested element. Accuracy and efficiency of the suggested element are compared with those of other strain-based plane elements. Detailed discussions are proposed after each benchmark problem. Finally, based on the attained results, a final conclusion about the characteristics of robust membrane elements is made.

1. Introduction

Numerical methods are proved to be powerful and effective computational tools for the analysis of complicated and practical engineering problems. Various numerical approaches were developed in the past decades such as the finite element method, finite difference technique, boundary element method, and discrete element approach. Among these techniques, the finite element method has obtained greater popularity due to its strong mathematical bases and inherent capabilities. Accordingly, various formulation techniques were developed in the past decades, and there are thousands of finite elements available to analyze different types of problems and structures. Among the available approaches to finite element formulation, the most well-known and widely applicable one is the displacement-based technique. This method, sometimes known with different terms, such as the classical or stiffness approach, is the first scheme that is used for the development of finite elements [1]. Clear and straightforward process and applicability to different types of problems and structures are the prominent advantages of the displacement-based formulation for structural and mechanical applications. However, this process has various shortcomings. For instance, inaccuracy and discontinuity of stresses, which are secondary parameters in the stiffness approach, represent vital deficiency in structural applications, where stress is a decisive parameter in the design practice. Another common problem of displacement-based finite elements includes various locking phenomena, such as shear and membrane locking, which necessitate special treating, often requiring considerable time and effort and reducing the efficiency of the method [2,3]. Moreover, in severely nonlinear problems, the displacement-based elements usually necessitate utilizing very fine meshes, which are inappropriate in terms of efficiency. To remedy the mentioned and other shortcomings of the displacement

*. *Corresponding author. Tel./Fax: +98 51 38412912*
E-mail addresses: Rezaiee@um.ac.ir (M. Rezaiee-Pajand); Nima.Gharaei@gmail.com (N. Gharaei-Moghaddam); Mohammadrezaramezani1994@gmail.com (MR. Ramezani)

doi: 10.24200/sci.2019.21429

approach, other finite element formulations, such as the force-based, hybrid or mixed, assumed stress, and assumed strain, have been developed. Fortunately, these new procedures have their own advantages and shortcomings. For example, the force-based formulation performs very well in the linear and nonlinear analyses of frame structures and, also, provides an appropriate platform for the development of advanced frame elements [4-8]. Of note, the force formulation approach is limited to skeletal structures, and its application to continuous structures is very difficult if not possible. Despite the fact that each method has different merits and limitations, some approaches have received greater attention from researchers, while others have been almost overlooked. One of these techniques that has received less attention despite its promising performance is the strain-based or assumed strain approach. It is proved that the strain-based approach is very effective in removing problems such as shear parasitic error, mesh sensitivity, and different locking phenomena. Various authors have utilized this scheme to develop strain-based plane elements [9-26]. Sabir is one of the pioneers of the development of strain formulation. In his early work, he proposed triangular and quadrilateral elements by assuming linear strain fields [9]. In another work, Sabir and Sfendji proposed four-node triangular and rectangular elements by assuming the linear normal strains and constant shear strain [10]. In 2003, Tayeh developed new strain-based triangular and rectangular elements using a higher-order incomplete second-order field for the element [11]. Belarbi and Bourezane proposed a new element by incorporating Poisson's ratio in the assumed strain field [12]. Belarbi and Bourezane performed another study in 2005 and proposed a triangular strain-based element with the geometry similar to their previous work, yet with a different strain field [13]. In 2005, Belarbi and Maalem suggested an improved strain-based rectangular element by considering linear normal strains and constant shear strain [14]. The first generalized quadrilateral plane element, whose strain field satisfies both compatibility and equilibrium conditions, was proposed by Rezaiee-Pajand and Yaghoobi [15]. In another study, Rezaiee-Pajand and Yaghoobi investigated the performance of two special rectangular variants of the previous element [16]. A four-node rectangular strain-based element with incomplete fourth-order normal strains was proposed by Rebiai and Belounar [17]. Rezaiee-Pajand and Yaghoobi proposed a five-node triangular element with a complete linear strain field [18]. To propose a new finite element, they utilized the complete linear strain field of the previous study, yet with an element of different geometry [19]. In another research work, Rebiai and Belounar suggested a variant of their previous element [20]. They considered the strain field of their previous study [17], yet added a new linear term to the shear strain and changed the dependent term of the normal strains. Following his previous research studies, Rebiai et al. suggested a new strain-based quadrilateral element for linear dynamic analysis of the plane problems [21]. In an attempt to develop second-order strain-based elements, Rezaiee-Pajand and Yaghoobi proposed two quadrilateral strain-based elements with seven and nine nodes [22]. In 2016, Hamadi et al. independently proposed a new quadrilateral finite element [23]. This element is exactly similar to the element previously proposed by Rezaiee-Pajand and Yaghoobi in 2012 [15]. In order to analyze geometrically nonlinear plane structures, Rezaiee-Pajand and Yaghoobi modified their five-node quadrilateral element [15] by the co-rotational approach [24]. In a more recent attempt to propose a three-node nine-degree-of-freedom triangular element, Rebiai suggested a new strain-based element with an incomplete second-order strain field [25]. Rezaiee-Pajand carried out various studies to improve the performance of the strain-based finite elements. In one of the most recent studies, He and Gharaei-Moghaddam and Ramezani suggested new triangular elements [26]. Moreover, they also imposed the equilibrium condition to specify the dependent strain states. In addition to the mentioned plane elements, advantages of strain formulation persuade researchers to make use of this approach to develop finite elements of other types of structures [27-42].

A review of the existing strain-based plane elements shows that there is no membrane element with a complete second-order assumed strain field, despite the fact that the application of higher-order fields leads to highly accurate estimation. Moreover, it is known that the use of complete strain fields in element formulation guarantees locking-free behavior for strain-based elements [15]. Therefore, in the present study, a new second-order strain-based element is proposed to investigate the effect of higher-order strain states and a new distribution model for degrees of freedom on the accuracy of the resulting element. The mentioned benchmark problems are resolved using the new element. Based on the obtained results by the suggested element and the reviewed membrane elements, a short discussion is provided after each problem. The attained results can be used to detect the most suitable assumptions and configurations to achieve a robust plane finite element.

2. Basics of the formulation

The main idea of the assumed strain formulation is to approximate the strain field of the element with an assumed mathematical function. Polynomial Taylor expansion is a common choice for the assumed function. In the case of plane problems, the strain field consists of

$$\begin{cases} \varepsilon_x(x,y) = (\varepsilon_x)_0 + (\varepsilon_{x,x})_0 x + (\varepsilon_{x,y})_0 y + (\varepsilon_{x,xx})_0 \left(\frac{x^2}{2}\right) + (\varepsilon_{x,xy})_0 (xy) + (\varepsilon_{x,yy})_0 \left(\frac{y^2}{2}\right) + ... \\ \varepsilon_y(x,y) = (\varepsilon_y)_0 + (\varepsilon_{y,x})_0 x + (\varepsilon_{y,y})_0 y + (\varepsilon_{y,xx})_0 \left(\frac{x^2}{2}\right) + (\varepsilon_{y,xy})_0 (xy) + (\varepsilon_{y,yy})_0 \left(\frac{y^2}{2}\right) + ... \\ \gamma_{xy}(x,y) = (\gamma_{xy})_0 + (\gamma_{xy,x})_0 x + (\gamma_{xy,y})_0 y + (\gamma_{xy,xx})_0 \left(\frac{x^2}{2}\right) + (\gamma_{xy,xy})_0 (xy) + (\gamma_{xy,yy})_0 \left(\frac{y^2}{2}\right) + ... \end{cases} \tag{1}$$

Box I

three components, namely ε_x, ε_y, and γ_{xy}. According to the concept of Taylor expansion, each of the strain components can be approximated by a polynomial function of arbitrary order in the form of Eq. (1) shown in Box I. Choosing the higher-order terms of Taylor expansion for the assumed strain field would increase convergence speed and accuracy of the suggested element and, yet, reduce its numerical efficiency due to the addition of more degrees of freedom to the element. Despite the application of different criteria, such as pure plain bending test, for choosing the higher-order terms for strain components, there is no required condition for this selection, and the only necessity is to include constant terms in the assumed strain field. However, like the classical displacement-based formulation, it is advised not to assign priority to any of the coordinates (x or y). Moreover, it is possible to select strain components of specific order according to the knowledge of analytic form of the strain field.

In any case, when the desired terms are chosen for the strain components, it is possible to apply any preferred optimized condition to the assumed strain field. These optimized criteria provide necessary or favorite properties for the element strain field. The most common criteria include compatibility and equilibrium conditions. Based on the plane elasticity principle, the compatibility of the strain field is satisfied, provided that the following relationship is established between the strain components:

$$\frac{\partial^2 \varepsilon_x}{\partial y^2} + \frac{\partial^2 \varepsilon_y}{\partial x^2} = \frac{\partial^2 \gamma_{xy}}{\partial x \partial y}. \tag{2}$$

The other common optimized condition is equilibrium. The equation of equilibrium for the plane problems is defined as follows:

$$\begin{cases} \frac{\partial \sigma_x}{\partial x} + \frac{\partial \tau_{xy}}{\partial y} + F_x = 0 \\ \frac{\partial \sigma_y}{\partial y} + \frac{\partial \tau_{xy}}{\partial y} + F_y = 0 \end{cases} \tag{3}$$

where F_x and F_y are the body forces in x and y directions, respectively. σ_x, σ_y, and τ_{xy} are normal and shearing stresses, respectively. To rewrite the equilibrium equation in terms of strain, it is necessary to relate the stresses to the strains. For the plane problems, the coming relations connect stresses and strains to each other:

$$\begin{cases} \sigma_x = 2G\varepsilon_x + \lambda(\varepsilon_x + \varepsilon_y) \\ \sigma_x = 2G\varepsilon_y + \lambda(\varepsilon_x + \varepsilon_y) \\ \tau_{xy} = G\gamma_{xy} \end{cases} \tag{4}$$

λ is called the Lame constant and is equal to $\frac{\nu E}{(1+\nu)(1-\nu)}$ for the plane stress condition. In the case of plane strain, this constant is equal to $\frac{\nu E}{(1+\nu)(1-2\nu)}$. E, G, and ν are the modulus of elasticity, shear modulus, and Poisson's ratio, respectively. Substituting Eq. (4) in the equilibrium equation results in the following relations:

$$\begin{cases} (2G+\lambda)\frac{\partial \varepsilon_x}{\partial x} + \lambda \frac{\partial \varepsilon_y}{\partial x} + G\frac{\partial \gamma_{xy}}{\partial y} + F_x = 0 \\ \lambda \frac{\partial \varepsilon_x}{\partial y} + (2G+\lambda)\frac{\partial \varepsilon_y}{\partial y} + G\frac{\partial \gamma_{xy}}{\partial x} + F_y = 0 \end{cases} \tag{5}$$

The inclusion of the optimized condition makes some of the strain states dependent on the other ones. When the dependent strain states are determined, the assumed strain field is rewritten in terms of the independent ones. The next step is to calculate the associated displacement field. For this purpose, the strain-displacement formulae are utilized:

$$\begin{cases} \varepsilon_x = \frac{\partial u}{\partial x} \\ \varepsilon_y = \frac{\partial v}{\partial y} \\ \varepsilon_x = \frac{1}{2}\left(\frac{\partial u}{\partial y} + \frac{\partial v}{\partial x}\right) \end{cases} \tag{6}$$

In these relations, u and v are displacements in x and y directions, respectively. Based on these equalities, the displacements in x and y directions are derived by integrating normal strain components with respect to their associated coordinates:

$$\begin{cases} u(x,y) = \int \varepsilon_x dx + f_1(y) \\ v(x,y) = \int \varepsilon_y dx + f_2(y) \end{cases} \tag{7}$$

In these equations, f_1 and f_2 are derived by integrating shear strain with respect to the coordinates and imposing necessary conditions of the rigid body modes. For a plane problem, there are three rigid body modes in the displacement field, namely u_o, v_o, and r_o, standing for rigid body displacements in x and y directions and rigid body rotation, respectively. According to the displacement-based formulation, the existence of these terms is a necessary condition to guarantee the convergence of the resulting finite element. Therefore, these modes are also counted among the independent strain states that can be arranged in a vector arrangement indicated by S. This vector is called strain state vector. By using the matrix notation which is traditionally used in finite element formulation in structural engineering applications, it is possible to relate the displacement and strain fields to the strain state vector in the subsequent forms:

$$U = N_S.S + \widetilde{U}, \tag{8}$$

$$\varepsilon = B_S.S + \widetilde{\varepsilon}, \tag{9}$$

where N_S and B_S are displacement and strain interpolation matrices, respectively. $\widetilde{U}$ and $\widetilde{\varepsilon}$ are particular part of the displacement and strain fields that depend on the body forces. The element nodal displacements can be computed by substituting coordinates of the element nodes in the displacement field. Thus, the following relation can be established between the vectors of nodal displacements and the strain states:

$$D = A.S + \widetilde{D} = \overline{D} + \widetilde{D}. \tag{10}$$

In this equation, D and $\widetilde{D}$ are the nodal displacement vectors due to body forces. A is the geometric matrix, which consists of the nodal displacement interpolation matrices of the element. By considering Eq. (10), it is possible to construct the succeeding relations between the displacement and strains fields of the element with the nodal displacement vector:

$$\begin{aligned} U &= N_S.S + \widetilde{U} = N_S.\left(A^{-1}.\overline{D}\right) + \widetilde{U} \\ &= \left(N_S.A^{-1}\right)\overline{D} + \widetilde{U} = N.\overline{D} + \widetilde{U}, \end{aligned} \tag{11}$$

$$\begin{aligned} \varepsilon &= B_S.S + \widetilde{\varepsilon} = B_S.\left(A^{-1}.\overline{D}\right) + \widetilde{\varepsilon} \\ &= \left(B_S.A^{-1}\right)\overline{D} + \widetilde{\varepsilon} = B.\overline{D} + \widetilde{\varepsilon}. \end{aligned} \tag{12}$$

Because the body forces are usually negligible in comparison with the applied loads, the strains and displacements due to body forces, $\widetilde{\varepsilon}$ and $\widetilde{U}$, are neglected.

The last step in the formulation of the finite element scheme is to derive the element stiffness matrix and the nodal force vector. There are different approaches to finding the stiffness matrix of an element. For instance, it is possible to utilize the total potential energy principle. This functional can be written as follows:

$$\Pi = \frac{1}{2}\int \sigma^T \varepsilon dv - \int U^T F dv - D^T P_{ext}. \tag{13}$$

In this relation, P_{ext} and F are the applied external nodal and body forces, respectively. To derive the element stiffness matrix and nodal force vector, it is required to establish a stationary of the functional:

$$\begin{aligned} \frac{\partial \Pi}{\partial \overline{D}} =& A^{-T}\left(\int B_S^T.D_m.B_S dv\right) A^{-1}.\overline{D} \\ & - A^{-T}\left(\int N_S^T.F dv\right) - P_{ext} = K\overline{D} - P = 0. \end{aligned} \tag{14}$$

Accordingly, the element stiffness matrix and nodal force vector are derived as follows:

$$K = A^{-T}\left(\int B_S^T.D_m.B_S dv\right) A^{-1} = A^{-T}.K_0.A^{-1}, \tag{15}$$

$$P = P_{ext} + A^{-T}\left(\int N_S^T.F dv\right), \tag{16}$$

where D_m is the material matrix:

$$D_m = \frac{E}{1-\nu^2}\begin{bmatrix} 1 & \nu & 0 \\ \nu & 1 & 0 \\ 0 & 0 & \frac{1-\nu}{2} \end{bmatrix}. \tag{17}$$

3. Element formulation

To propose a new strain-based membrane element, it is assumed that the normal strains have complete second-order field, while the shear strain is approximated using a linear field as shown in Box II.

It is proved that the imposition of compatibility and equilibrium conditions on the assumed strain field results in a more accurate element with a faster convergence trend [15]. Moreover, this action reduces the number of independent strain states in the element strain field. The number of independent strain states specifies the number of required degrees of freedom; therefore, their reduction results in an element with fewer degrees of freedom, which is more desirable from a numerical efficiency standpoint. Accordingly, enforcing the compatibility and equilibrium criteria on the assumed strain field of Eq. (18) (shown in Box II)

$$\begin{cases} \varepsilon_x(x,y) = (\varepsilon_x)_0 + (\varepsilon_{x,x})_0 x + (\varepsilon_{x,y})_0 y + (\varepsilon_{x,xx})_0\left(\frac{x^2}{2}\right) + (\varepsilon_{x,xy})_0 (xy) + (\varepsilon_{x,yy})_0\left(\frac{y^2}{2}\right) \\ \varepsilon_y(x,y) = (\varepsilon_y)_0 + (\varepsilon_{y,x})_0 x + (\varepsilon_{y,y})_0 y + (\varepsilon_{y,xx})_0\left(\frac{x^2}{2}\right) + (\varepsilon_{y,xy})_0 (xy) + (\varepsilon_{y,yy})_0\left(\frac{y^2}{2}\right) \\ \gamma_{xy}(x,y) = (\gamma_{xy})_0 + (\gamma_{xy,x})_0 x + (\gamma_{xy,y})_0 y \end{cases} \tag{18}$$

Box II

results in the subsequent dependent strain states:

$$\begin{cases}(\varepsilon_{y,xy})_0 = 0\\ (\varepsilon_{y,xx})_0 = -(\varepsilon_{x,yy})_0\\ (\gamma_{xy,y})_0 = -\frac{2G+\lambda}{G}(\varepsilon_{x,x})_0 - \frac{\lambda}{G}(\varepsilon_{y,x})_0\\ (\gamma_{xy,x})_0 = -\frac{2G+\lambda}{G}(\varepsilon_{y,y})_0 - \frac{\lambda}{G}(\varepsilon_{x,y})_0\\ (\varepsilon_{x,xy})_0 = -\frac{\lambda}{2G+\lambda}(\varepsilon_{y,xy})_0\\ (\varepsilon_{y,yy})_0 = -\frac{\lambda}{2G+\lambda}(\varepsilon_{x,yy})_0\\ (\varepsilon_{x,xx})_0 = \frac{\lambda}{2G+\lambda}(\varepsilon_{x,yy})_0\end{cases} \tag{19}$$

The assumed strain field in Eq. (18) consists of fifteen strain states, which, in addition to three rigid body modes, results in a total of eighteen strain states. As presented by Eq. (19), seven of these strain states are dependent on the others; therefore, the element strain state vector consists of eleven constituents as follows:

$$S=\left\{u_0 \quad v_0 \quad r_0 \quad (\varepsilon_x)_0 \quad (\varepsilon_y)_0 \quad (\gamma_{xy})_0 \quad (\varepsilon_{x,x})_0 \quad (\varepsilon_{x,y})_0 \right.$$

$$\left. (\varepsilon_{y,x})_0 \quad (\varepsilon_{y,y})_0 \quad (\varepsilon_{x,yy})_0 \right\} \tag{20}$$

where u_o, v_o, and r_o are the rigid body motions. By using this vector, the assumed strain field of the element can be rearranged in the succeeding matrix notations:

$$\varepsilon = B_S.S, \tag{21}$$

where the strain interpolation matrix, B_S, is defined by Eq. (22) as shown in Box III.

By utilizing the strain-displacement relations and performing integration of the strain components, the element displacement field in terms of independent strain states and rigid body modes is obtained. The displacement field can be reported using matrix notations:

$$U = N_S.S, \tag{23}$$

where the displacement interpolation matrix is presented by Eq. (24) as shown in Box IV. The next step of the formulation is to select element geometry and degrees of freedom.

First of all, it is required to determine the geometry of the element. Since many of the available plane elements formulated by various methods are quadrilateral, it is preferred to suggest robust triangular element. Moreover, triangular geometry facilitates meshing of structures of different shapes. Regarding the type of the degrees of freedom, for the new element, both translational and drilling degrees of freedom will be used. It is well known that the addition of drilling degrees of freedom to membrane elements is beneficial because of three main reasons: (a) It facilitates the development of shell elements and connection of shell and membrane element to beam elements, (b) The drilling degrees of freedom can be added to the element without the necessity of adding new mid-side nodes, and (c) It is effortless to include these extra degrees of freedom in the commercial finite element programs, which usually can carry six degrees of freedom per node [43]. Moreover, various studies showed that, in addition to the mentioned advantages, using drilling degrees of freedom improved the performance of membrane elements, especially under bending loads [44-48], and this is the main reason for using drilling degrees of freedom in the formulation of the new strain-based element in the present study. However, since the author's goal is to investigate effects of node distribution and the type of degrees of freedom on the performance of strain-based element, the second mentioned advantage of using drilling degrees of freedoms is violated and, instead, drillings are considered for new mid-side nodes. This assumption results in a new element configuration, which is not treated previously by researchers. This element is demonstrated in Figure 1. As can be seen, the element had seven nodes and eleven degrees of freedom in agreement with the independent strain

$$B_S = \begin{bmatrix} 0 & 0 & 0 & 1 & 0 & 0 & x & y & 0 & 0 & \frac{y^2}{2} + \frac{\lambda x^2}{2(2G+\lambda)} \\ 0 & 0 & 0 & 0 & 1 & 0 & 0 & 0 & x & y & -\frac{x^2}{2} + \frac{\lambda y^2}{2(2G+\lambda)} \\ 0 & 0 & 0 & 0 & 0 & 1 & -\frac{(2G+\lambda)y}{G} & -\frac{\lambda}{G}x & -\frac{\lambda}{G}y & -\frac{(2G+\lambda)x}{G} & 0 \end{bmatrix}. \tag{22}$$

Box III

$$N_S = \begin{bmatrix} 1 & 0 & -y & x & 0 & \frac{y}{2} & \frac{x^2}{2} - \frac{(2G+\lambda)y^2}{2G} & xy & -y^2\left(\frac{G+\lambda}{2G}\right) & 0 & -\frac{x^3}{6}\left(\frac{\lambda}{2G+\lambda}\right) + \frac{xy^2}{2} \\ 0 & 1 & x & 0 & y & \frac{x}{2} & 0 & -x^2\left(\frac{G+\lambda}{2G}\right) & xy & \frac{y^2}{2} - \frac{(2G+\lambda)x^2}{2G} & -\frac{y^3}{6}\left(\frac{\lambda}{2G+\lambda}\right) + \frac{yx^2}{2} \end{bmatrix}. \tag{24}$$

Box IV

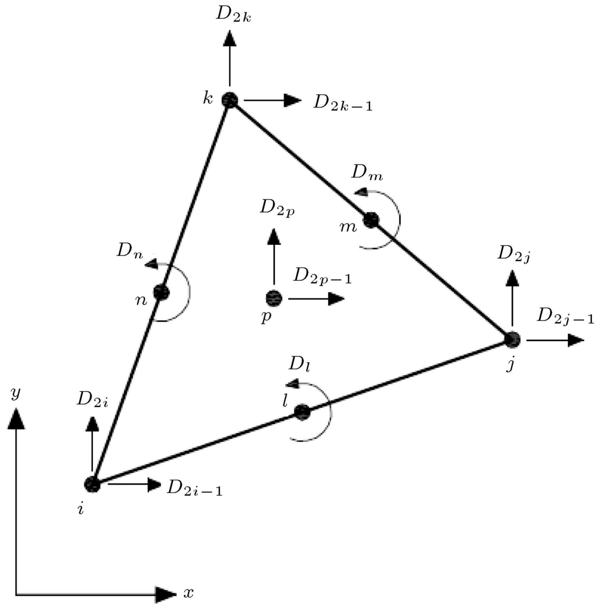

Figure 1. Seven-node triangular element with an incomplete second-order strain field.

states. The nodal displacement vector can be written as follows:

$$D = \{D_{2i-1} \;\; D_{2i} \;\; D_{2j-1} \; D_{2j} \;\; D_{2k-1} \;\; D_{2k} \;\; D_l \;\; D_m \;\; D_n \;\; D_{2p-1} \;\; D_{2p}\}^T. \tag{25}$$

The drilling degree of freedom is related to displacement components by the following equation:

$$\theta = \frac{1}{2}\left(\frac{\partial v}{\partial x} - \frac{\partial u}{\partial y}\right). \tag{26}$$

Therefore, it is possible to calculate drilling in terms of strain states vector as shown in Box V. The required quantity for the element formulation is the geometric matrix. According to Figure 1 and the selected degrees of freedom, the geometric matrix of this element is derived from the subsequent relation:

$$A = [N_{si} \quad N_{sj} \quad N_{sk} \quad T_{sl} \quad T_{sm} \quad T_{sn} \quad N_{sp}]^T. \tag{29}$$

Now, the element stiffness matrix and the vector of nodal forces can be computed by Eqs. (15) and (16). The accuracy and efficiency of the suggested element will be evaluated in the following section using a series of well-known benchmark problems. Moreover, the attained results reported by other researchers who proposed assumed strain membrane elements are also presented to provide an opportunity for comparison.

4. Numerical evaluation

In this section, a series of benchmark problems are solved to evaluate the performance of the suggested element. Table 1 presents a list of the strain-based elements used for comparison. In addition to the listed elements, results of the three common displacement-based elements, namely four-node and eight-node isoparametric quadrilateral elements (Q4 and Q8) and Linear Strain Triangular element (LST), are provided in some problems to compare the performance of the strain-based formulation with them.

4.1. Cantilever beam with distorted mesh

One of the available tests to examine the performance of the membrane elements in coarse distorted meshes under both bending and shear loadings is the cantilever beam, which is depicted in Figure 2.

This figure illustrates the geometric characteristics, loading, and utilized meshes for quadrilateral elements. The modulus of elasticity and Poisson's ratio of this beam are 1500 and 0.25, respectively, and its thickness is equal to 1. The utilized mesh for analysis using triangular elements is demonstrated in Figure 3.

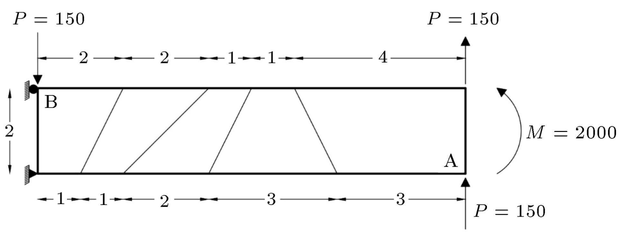

Figure 2. Cantilever beam with distorted quadrilateral mesh.

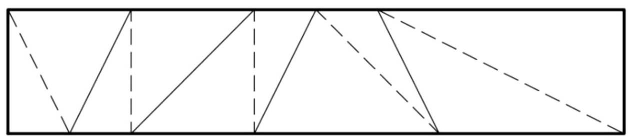

Figure 3. Triangular mesh for analysis of cantilever beam with distorted mesh.

$$\theta = T_s.S, \tag{27}$$

$$T_s = \left[0 \quad 0 \quad 1 \quad 0 \quad 0 \quad 0 \quad \tfrac{(2G+\lambda)y}{2G} \quad \tfrac{-(2G+\lambda)x}{2G} \quad \tfrac{(2G+\lambda)y}{2G} \quad \tfrac{-(2G+\lambda)x}{2G} \quad -xy\right]. \tag{28}$$

Box V

Table 1. List of the plane elements used for comparison.

No.	Abbreviation	Description of the element	Reference
		Triangular elements	
1	RY-T10	Six-node ten-degree-of-freedom triangular element proposed by Rezaiee-Pajand and Yaghoobi	[18]
2	RY-T10D	Seven-node ten-degree-of-freedom triangular element with drilling proposed by Rezaiee-Pajand and Yaghoobi	[19]
3	R-T9D	Three-node nine-degree-of-freedom triangular element with drilling proposed by Rebiai	[25]
4	RGR-T10	Five-node ten-degree-of-freedom triangular element proposed by Rezaiee-Pajand et al.	[26]
5	RGR-T10D	Four-node ten-degree-of-freedom triangular element with drilling proposed by Rezaiee-Pajand et al.	[26]
		Quadrilateral elements	
1	RY-Q10	Five-node ten-degree-of-freedom quadrilateral element proposed by Rezaiee-Pajand and Yaghoobi	[15]
2	RY-R10-I	First five-node ten-degree-of-freedom rectangular element proposed by Rezaiee-Pajand and Yaghoobi	[16]
3	RY-R10-II	Second five-node ten-degree-of-freedom rectangular element proposed by Rezaiee-Pajand and Yaghoobi	[16]
4	RB-R12D	Four-node twelve-degree-of-freedom rectangular element with drilling proposed by Rebiai and Belounar	[17]
5	RB-Q12D	Four-node twelve-degree-of-freedom quadrilateral element with drilling proposed by Rebiai and Belounar	[20]
6	RSB-Q12D	Four-node twelve-degree-of-freedom quadrilateral element with drilling proposed by Rebiai et al.	[21]
7	RY-Q14D	Five-node fourteen-degree-of-freedom quadrilateral element with drilling proposed by Rezaiee-Pajand and Yaghoobi	[22]
7	RY-Q18	Nine-node eighteen-degree-of-freedom quadrilateral element proposed by Rezaiee-Pajand and Yaghoobi	[22]

As evident, each quadrilateral element is divided by a dashed line to two triangular elements.

The attained results by the proposed element and other elements for deflection of point A and normal stress at point B are listed in Table 2.

In fact, this test measures the performance of different elements to analyze structures with distorted meshes under bending and shear loading conditions. According to the results, the proposed strain-based element provides acceptable accuracy. The results were obtained by RGR-T10 and RGR-T10D with the same assumed strain field, and their difference was only observed in terms of distribution. The type of degrees of freedom verifies this conjecture including drilling degrees of freedom in the plane elements and improves their performance under in-plane bending.

Table 2. Deflection of point A and stress at point B of the cantilever beam with distorted mesh.

Element		Load P		Load M	
		Vertical Displacement of point A	**Stress at point B**	**Vertical Displacement of point A**	**Stress at point B**
Quadrilateral elements	Q8	100.40	−3354	98.40	−2428
	Q4	50.70	−2448	45.70	−1761
	SSQUAD	102.79	—	100.00	—
Triangular elements	RGR-T10	103.65	−4213	98.50	−2832
	RGR-T10D	101.83	−4020	100.00	−3000
	Proposed element	**103.92**	**−4081**	**100.70**	**-2983**
Analytical solution		102.60	−4050	100.00	−3000

4.2. Cantilever beam under parabolic shear loading

To investigate the performance of the elements in analyzing structures under distributed surface traction, the cantilever beam demonstrated in Figure 4 is analyzed. This beam is made of elastic material with modulus of elasticity and Poisson's ratio equal to 3000 and 0.25, respectively, and its thickness is taken to be 1 unit. The beam is loaded by parabolic distributed traction at its free end, which is equal to 40 units.

This benchmark problem evaluates the efficiency of the elements in the analysis of structures using coarse meshes. As evident in Figure 4, the beam is discretized by four quadrilateral elements. In the case of triangular elements, eight elements are used in which the utilized mesh is demonstrated in Figure 5. However, results of some of the reviewed elements are reported for regular mesh.

Table 3 presents the obtained responses by the mentioned membrane elements for deflections at the tip of the beam. Felippa reported the near-exact tip deflection of the beam equal to 0.35601 [49].

Based on the reported results, RGR-T10 and RY-Q14D are the most accurate elements in this problem with only 0.03% error in their estimations. The suggested element in this study is in the second place with less than 1% error.

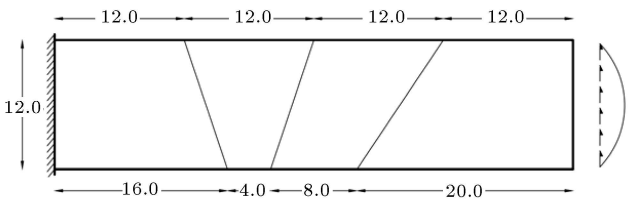

Figure 4. Cantilever beam under parabolic shear loading.

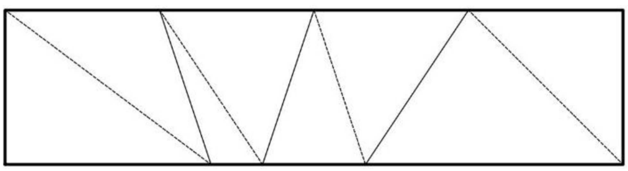

Figure 5. Triangular mesh for analysis of cantilever beam under parabolic shear loading.

4.3. Cook's skew beam

Cook trapezoidal beam is one of the most fundamental tests for checking shear displacements in non-rectangular geometry. Figure 6 demonstrates this beam under uniformly distributed tip loading. This beam has unit thickness and is made of materials whose Young's modulus and Poisson's ratio are 1 and 1/3, respectively.

Many researchers have also implemented this

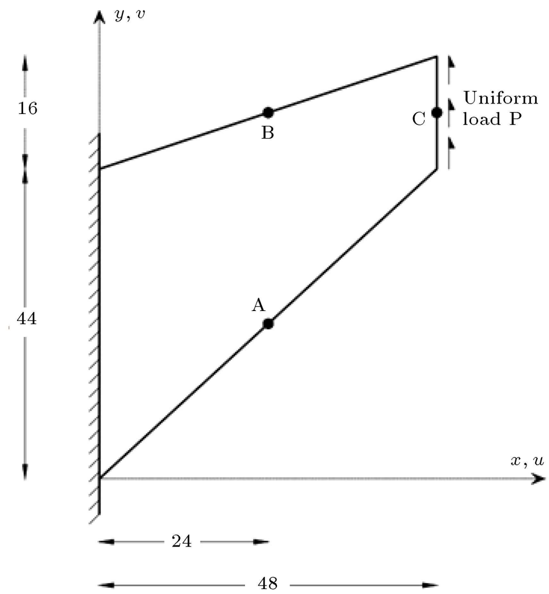

Figure 6. Cook's skew beam under uniform tip loading.

Table 3. Tip deflection of cantilever beam under parabolic shear.

	Element	Vertical displacement	Relative error
Quadrilateral elements	Q4	0.21290	−40.19
	Q8	0.34790	−2.28
	RY-Q10	0.35280	−0.90
	RY-R10-I	0.32724*	−8.08
	RY-R10-II	0.33027*	−7.23
	RB-R12D	0.34120*	−4.16
	RSB-Q12D	0.33470*	−5.98
	RY-Q14D	0.35590	−0.03
	RY-Q18	0.35230	−1.04
Triangular elements	LST	0.34770	−2.33
	RY-T10	0.35031*	−1.60
	RY-T10D	0.34680	−2.59
	RGR-T10	0.35610	0.03
	RGR-T10D	0.34680	−2.59
	Proposed element	**0.35850**	**0.70**
Near-exact solution		0.35601	

*The results are attained from a regular mesh.

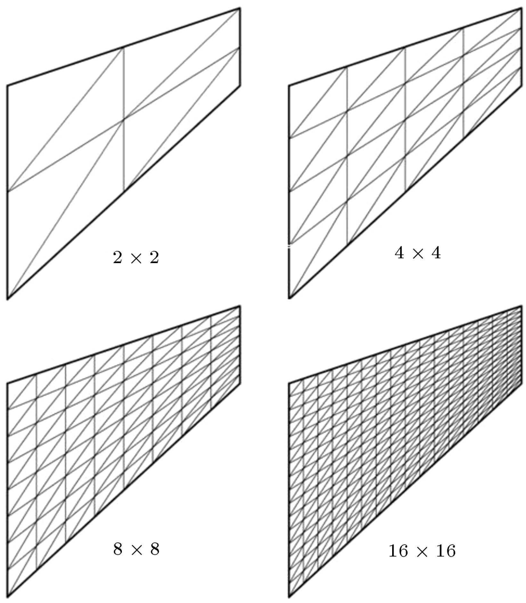

Figure 7. Utilized meshes for analysis of Cook's skew beam.

Table 4. Deflection of point C of the Cook's beam.

	Element	Mesh			
		2 × 2	4 × 4	8 × 8	16 × 16
Quadrilateral elements	Q4	11.80	18.29	22.08	23.43
	RY-Q10	25.65	24.27	24.01	23.96
	RB-Q12D	17.87	23.37	23.38	23.50
	RY-Q14D	27.61	30.48	31.85	32.44
	RY-Q18	23.45	23.70	23.86	23.92
Triangular elements	RY-T10	20.94	23.84	24.18	24.13
	RY-T10D	25.82	27.19	27.23	27.09
	R-T9D	18.78	23.94	23.94	23.94
	RGR-T10	21.18	23.03	23.69	23.95
	RGR-T10D	19.06	22.85	23.14	23.87
	RGR-T11D	**26.00**	**24.39**	**24.01**	**23.97**
Near-exact solution			23.96		

benchmark to challenge the convergence of their elements. Here, four different meshes, namely meshes 2×2, 4×4, 8×8, and 16×16, are used. These meshes are demonstrated in Figure 7. The results of the deflection at point C are presented in Table 4. It should be noted that the near-exact solution to this problem is reported equal to 23.96 [49].

Outcomes of this problem are again in complete agreement with the findings of previous numerical examples and, once more, the proposed element is among the best performing elements. The other elements that provide accurate estimations are RY-Q10, RGR-T10, and R-T9D. It is somehow unexpected that R-T9D is able to compute a very accurate response by a very coarse mesh of 4×4. As is evident, the convergence trend of different elements is not similar. While most of the elements converge to the exact response asymptotically from below, the proposed element approaches the accurate response from above. In addition, there are elements such as RY-T10 and RY-T10D that show non-uniform convergence behavior and, even, RY-Q14D goes beyond the response. Nevertheless, most of the strain-based elements demonstrate reasonable performance in this benchmark problem.

4.4. Thick curved beam

In order to appraise the ability of finite elements, especially triangular ones, to analyze curvy structures, many of the previous researchers have evaluated performance of their proposed element in the analysis of the curved beams, as demonstrated in Figure 8. This beam is loaded by the shear load $P = 600$ at its tip.

The modulus of elasticity, poison's ratio, and thickness of this beam are 1000, 0, and 1, respectively. As depicted in Figure 8, four quadrilateral elements are used to mesh this structure. In the case of triangular elements, eight elements are used, as demonstrated in Figure 9.

The exact vertical displacement of point A under the applied load is equal to 90.10. The attained results by different elements are presented in Table 5. It is evident that the suggested element provides the most accurate estimation with only 0.24% error. After the proposed element, RGR-T10 with a relative error of 0.79% is in the second place. It is interesting to note that, among the quadrilateral elements, the performance of Q8 is better than those of the strain-based elements. Nonetheless, since the error of most of the strain-based elements is less than 5%, which is negligible by any set of standards for the utilized coarse mesh, this problem shows that the elements formulated by the assumed strain approach are suitable options for efficient analysis of curved structures and can compete with isoparametric elements.

Table 5. Deflection of point A of thick curved beam.

	Element	Load P	
		Vertical displacement	**Relative error**
Quadrilateral elements	Q8	88.60	−1.66
	RY-Q10	86.92	−3.53
	RY-Q14D	87.00	−3.44
	RY-Q18	86.45	−4.05
Triangular elements	RY-T10	87.15	−3.27
	RY-T10D	87.47	−2.92
	RGR-T10	89.39	−0.79
	RGR-T10D	84.62	−6.08
	RGR-T11D	**89.88**	**-0.24**
Analytical solution		90.10	

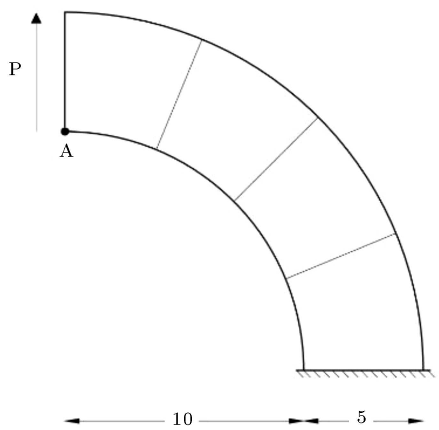

Figure 8. Thick curved beam with quadrilateral mesh.

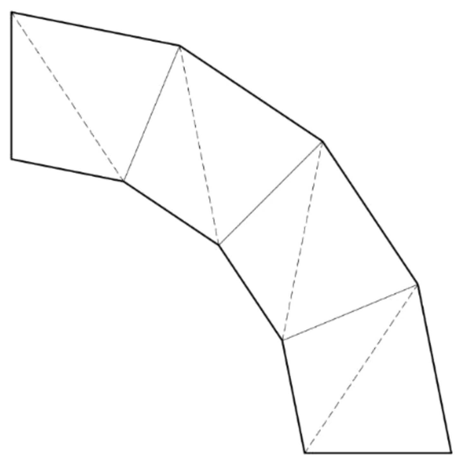

Figure 9. The triangular mesh for analysis of thick curved beam.

4.5. Thin curved beam

To investigate the effect of shear lock in curved structures and, also, the convergence rate to achieve a precise response, a thin curved beam test is available. This modulus of elasticity, poison's ratio, and thickness of this structure demonstrated in Figure 10 are 107, 0.25, and 0.1, respectively. This beam is loaded by a unit vertical force at its tip.

Three different meshes are used to analyze this structure, namely 1×6, 2×12, and 4×24. These meshes are named based on the number of quadrilateral elements used in them. Of note, to analyze using triangular elements, each quadrilateral element is divided into two triangular elements. For instance, 1×6 is demonstrated in Figure 11.

The main purpose of solving this problem is to

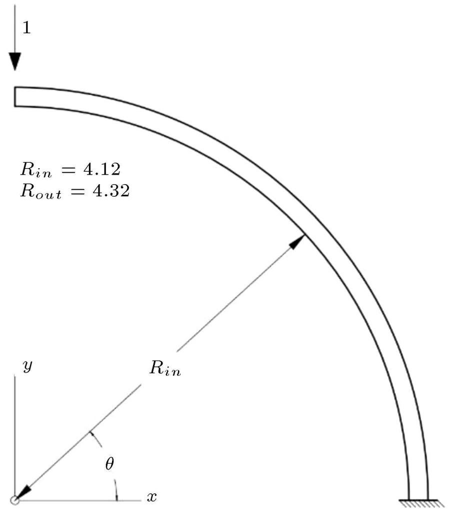

Figure 10. Thin curved beam.

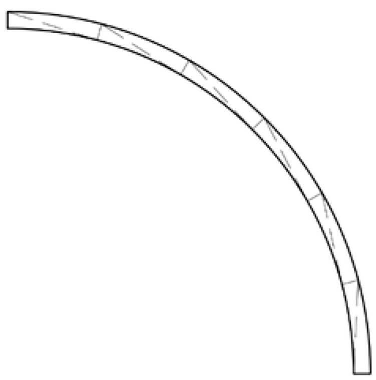

Figure 11. The used 1 × 6 mesh for analysis of thin curved beam.

compute tip deflection of the beam under applied load and, therefore, investigate the effect of locking problem on the performance of the strain-based elements. The exact vertical displacement at the tip is reported as equal to 0.08734 [15]. Table 6 presents the obtained results by some of the strain-based elements.

It is evident that the mentioned triangular elements, except the proposed one, face the locking problem in the coarsest mesh and behave too stiffly. In contrast, the proposed element provides an acceptable response. In the coarsest mesh, the suggested element does not lock and only has 5.07% error. This error is reduced to 0.49% in the finest mesh. Of note, the quadrilateral elements provide more accurate estimations in the coarse mesh; however, they become a bit more flexible in the finest mesh and, therefore, go beyond the exact solution.

4.6. McNeal's beam

McNeal and Harder proposed this benchmark to examine the sensitivity of the elements to the mesh distortion and the trapezoidal locking phenomenon [46]. The geometry of this beam and the rectangular, parallelogram, and trapezoidal meshes used for analysis by quadrilateral elements are depicted in Figure 12. The utilized meshes for triangular meshes are demonstrated in Figure 13.

Modulus of elasticity, poison's ratio, and thickness of the structure are 10^7, 0.3, and 0.1, respectively. Two modes of loading are assumed, as depicted in Figure 12. The derived responses by the strain-based elements are listed in Table 7.

This test is a difficult problem for many of the displacement-based membrane elements, since they demonstrate high sensitivity to trapezoidal meshes. For example, the powerful Q8 element with all of its capabilities faces fatal error for both modes of loading in trapezoidal mesh. However, as evident from the results presented in Table 7, most of the strain-based elements have no problem in this case.

4.7. Higher-order patch test

The beam, which is demonstrated in Figure 14, is the next numerical example that evaluates the performance of plane strain-based elements.

Table 6. Tip deflection of thin curved beam.

	Element	Mesh					
		1 × 6		2 × 12		4 × 24	
		Deflection	Error	Deflection	Error	Deflection	Error
Quadrilateral elements	RY-Q10	−0.08901	1.91	−0.08844	1.26	−0.08846	1.28
	RY-Q14D	−0.08748	0.16	−0.08898	1.87	−0.08925	2.19
	RY-Q18	−0.08745	0.12	−0.08840	1.21	−0.08850	1.33
Triangular elements	RY-T10	0.05634	−35.49	0.08491	−2.78	0.08815	0.93
	RGR-T10	−0.06305	−27.81	−0.08493	−2.76	−0.08609	−1.43
	RGR-T10D	−0.06486	−25.74	−0.08501	−2.67	−0.08650	−0.96
	RGR-T11D	**−0.08291**	**−5.07**	**−0.08434**	**−3.43**	**−0.08691**	**−0.49**
Analytical solution		-0.08734					

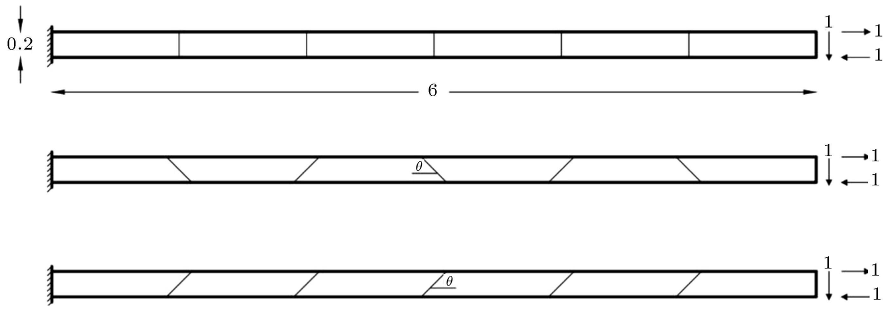

Figure 12. McNeal's beam and utilized quadrilateral meshes.

Table 7. Normalized tip deflection of the McNeal's beam.

	Element	Load P			Load M		
		Rectangular mesh	**Parallelogram mesh**	**Trapezoidal mesh**	**Rectangular mesh**	**Parallelogram mesh**	**Trapezoidal mesh**
Quadrilateral elements	Q4	9.30	3.58	3.06	9.34	3.14	2.21
	Q8	95.12	91.94	85.43	100.00	75.94	9.32
	RY-Q10	99.30	99.42	99.42	100.00	100.00	100.00
	RB-Q12D	99.26	98.69	98.78	99.63	99.26	99.26
	RSB-Q12D	100.00	97.59	97.78	100.00	98.89	98.89
	RY-Q14D	98.33	98.74	98.79	98.88	99.11	99.19
	RY-Q18	100.00	100.00	100.00	100.00	100.00	100.00
Triangular elements	LST	98.3	97.05	96.12	99.34	99.40	99.22
	RY-T10	99.44	94.30	92.11	100.00	100.00	100.01
	RY-T10D	99.43	94.94	92.31	100.00	100.00	100.00
	R-T9D	99.63	97.87	97.87	99.62	99.25	99.25
	RGR-T10	99.41	99.52	99.92	100.00	99.95	100.00
	RGR-T10D	99.33	94.12	90.56	100.00	99.98	100.00
	RGR-T11D	**104.34**	**102.48**	**104.99**	**100.79**	**100.56**	**100.94**
Analytical solutions			0.1081			0.0054	

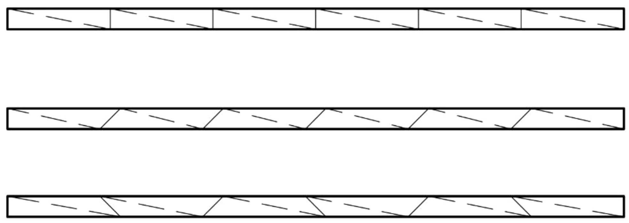

Figure 13. The utilized triangular meshes for analysis of McNeal's beam.

This beam with a geometric ratio of 10 is made of elastic material with modulus of elasticity and Poisson's ratio equal to 100 and 0, respectively. The thickness of the beam is taken as 1. Two different types of meshes, namely regular and distorted, are demonstrated in Figure 15 and are used.

This test examines the performance of the elements under the pure bending and considering the

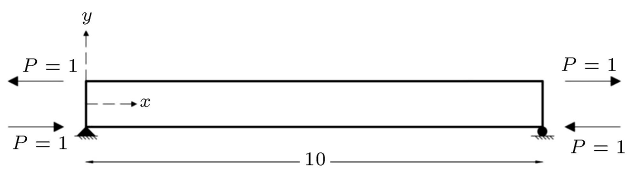

Figure 14. Higher-order patch test.

simple support conditions. The attained results by the strain-based elements are listed in Table 8. It is evident that, almost, all of the elements can compute the exact response regardless of the mesh type.

4.8. Thick-walled cylinder

The cylindrical plane strain test of the thick wall under uniform internal pressure is the eighth problem, which investigates the effect of Poisson's locking on the performance of strain-based elements. Due to symmetry,

Table 8. Maximum displacements of the higher-order patch test.

	Element	Regular mesh		Distorted mesh	
		Max U	Max V	Max U	Max V
Quadrilateral elements	RY-Q10	–0.600	1.500	–0.600	1.500
	RY-R10-I	–0.600	1.500	–0.600	1.500
	RB-R12D	–0.600	1.500	–0.600	1.500
	RB-Q12D	–0.594	1.493	–0.592	1.484
	RSB-Q12D	–0.590	1.500	–0.590	1.490
	RY-Q14D	–0.600	1.500	–0.600	1.500
	RY-Q18	–0.600	1.500	–0.600	1.500
Triangular elements	RY-T10D	–0.600	1.500	–0.600	1.500
	RGR-T10	–0.600	1.500	–0.600	1.500
	RGR-T10D	–0.600	1.500	–0.600	1.500
	RGR-T11D	**–0.600**	**1.500**	**–0.600**	**1.500**
Analytical solution		–0.600	1.500	–0.600	1.500

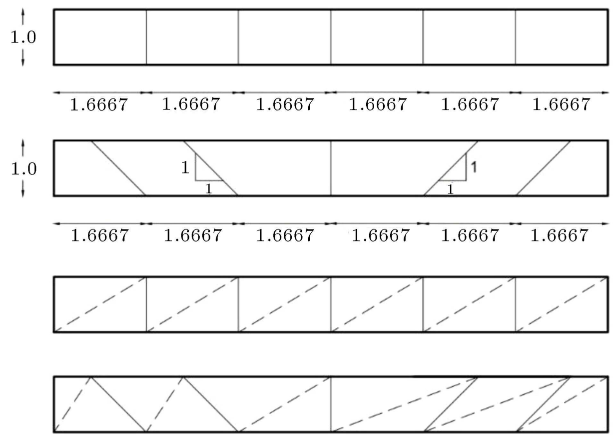

Figure 15. Utilized regular and distorted meshes.

only a quarter of this cylinder will be analyzed. This structure and utilized mesh are depicted in Figure 16.

The elastic modulus of the material is 1000, and it is solved for different values of Poisson's ratio varying from 0.3 to 0.4999. The exact radial displacements of this cylinder under internal pressure can be computed through the following relation [50]:

$$u_r = \frac{(1+\nu)pR_{in}^2}{E(R_{ex}^2 - R_{in}^2)}\left[\frac{R_{ex}}{r} + (1-2\nu)r\right], \tag{30}$$

where R_{in} and R_{ex} are the internal and external radii of the cylinder. The derived results by different elements are presented in Table 9. According to the outcomes, the assumed strain approach results in elements free from Poisson's locking.

4.9. Theoretical slender beam

The beam depicted in Figure 17 with a length of 100 is made of elastic material with Young's modulus and Poisson's ratio equal to 106 and 0.3, respectively. This structure is used to investigate the shear effect on the slender plane problems.

This structure is analyzed using two different meshes. The obtained results for tip displacements of

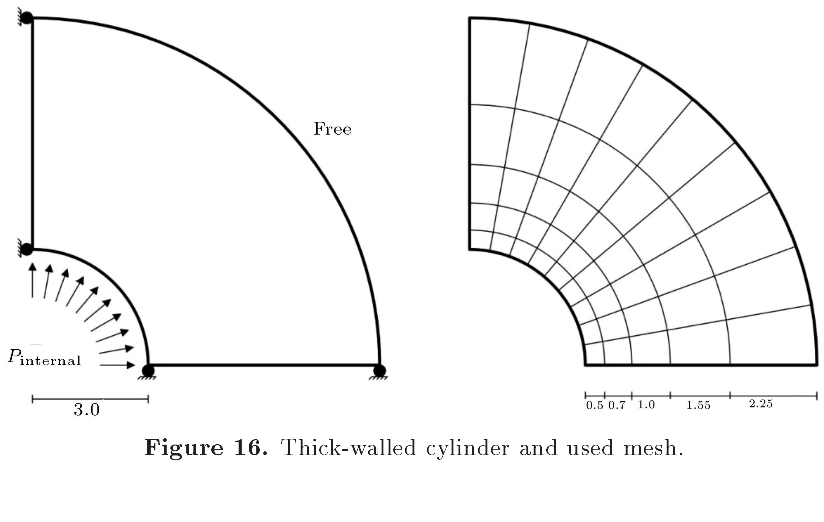

Figure 16. Thick-walled cylinder and used mesh.

Table 9. Normalized radial displacement of the thick walled cylinder at the inner radius.

Element		Poisson's ratio 0.3	0.49	0.499	0.4999
Quadrilateral elements	RY-Q10	0.9799	0.9789	0.9790	0.9794
	RY-Q14D	1.1805	1.1839	1.1841	1.1846
	RY-Q18	0.9360	0.9576	0.9593	0.9599
Triangular elements	**RGR-T11D**	**1.01869**	**1.0356**	**1.0361**	**1.0365**
Analytical solution		0.00506	0.00506	0.00504	0.00458

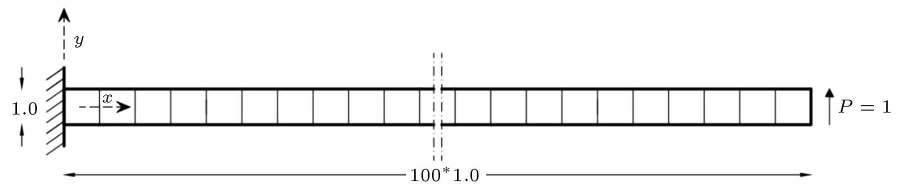

Figure 17. Extremely slender cantilever beam.

the beam are listed in Table 10. The proposed element and RGR-T10 have the best performance among the reported elements. It is evident that Q4 suffers from locking problem and, therefore, cannot compute exact response even using a fine mesh.

Table 10. Tip displacements of slender cantilever beam.

	Element	Mesh	Displacements $U_x \times 100$	U_y
Quadrilateral elements	Q4	1 × 100	2.0222	2.6965
		2 × 200	2.1280	2.8371
	RY-Q10	1 × 100	3.0046	4.0067
		2 × 200	2.9991	3.9982
	RY-R10-I	1 × 100	3.0046	4.0067
		2 × 200	2.9991	3.9982
	RY-R10-II	1 × 100	3.0000	4.0002
		2 × 200	2.9987	3.9976
	RY-Q14D	1 × 100	3.0000	4.0067
		2 × 200	3.193	4.2581
	RY-Q18	1 × 100	2.9983	3.9967
		2 × 200	2.9989	3.9980
Triangular elements	RY-T10	1 × 100	3.0000	4.0001
		2 × 200	2.9992	3.9986
	RGR-T10	1 × 100	3.0000	4.0000
		2 × 200	3.0000	4.0000
	RGR-T10D	1 × 100	2.9845	3.9767
		2 × 200	2.9944	3.9975
	RGR-T11D	**1 × 100**	**3.0001**	**4.0003**
		2 × 200	**3.0001**	**4.0001**
Analytical solution			3	4

4.10. Cantilever shear wall

An important purpose of formulating efficient elements is to analyze practical structures with minimal elements. Therefore, in order to investigate the efficiency of the strain-based elements in practical problems, two shear walls are examined with the proposed element and the other strain elements. In the first problem, the shear wall, which is shown in Figure 18, is analyzed.

The modulus of elasticity and Poisson's ratio of the wall are 2×10^7 and 0.2, respectively. Here, to reevaluate the accuracy and efficiency of strain formulation, as well as the potency of the proposed

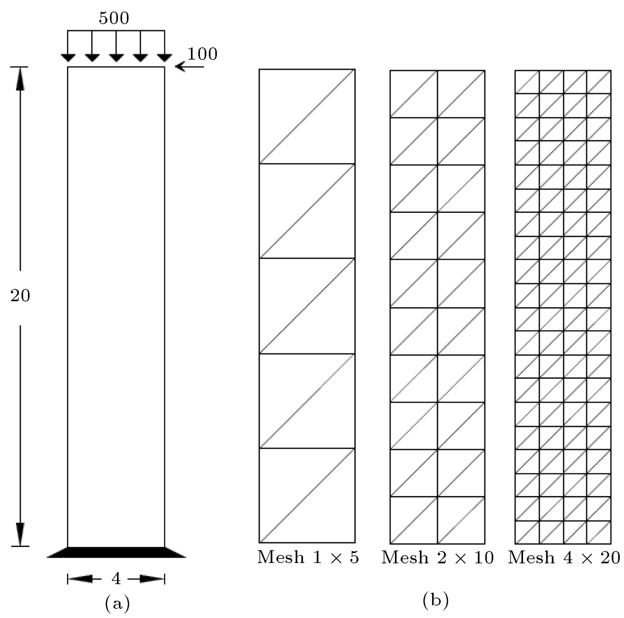

Figure 18. The shear wall and the utilized meshes.

Table 11. Lateral displacement of the top of the shear wall.

	Element	Mesh 1×5	2×10	4×20
Quadrilateral elements	Q8	62.17	80.10	89.17
	RY-R10-I	95.91	97.13	98.24
	RY-R10-II	95.87	96.99	98.19
	RY-Q14D	95.86	127.16	138.61
	RY-Q18	96.23	97.04	97.76
Triangular elements	RY-T10	96.86	97.53	98.35
	RGR-T10	96.62	97.78	98.12
	RGR-T10D	89.60	95.63	95.89
	RGR-T11D	**96.21**	**98.56**	**99.01**
Analytical solution			0.0025	

element, the conventional element Q8 is brought for comparison. Further, to investigate the convergence, two finer meshes have been used. The normalized responses are provided in Table 11.

Based on the results presented in Table 11, the suggested element demonstrates the best performance among the compared elements. Two interesting outcomes include lower accuracy of Q8 and inability of RY-Q14D, which becomes too flexible when using finer meshes. As can be observed, all of the reported strain-based elements except RGR-T10D have less than 5% error in their estimations when a coarse 1×5 mesh is used. This finding again demonstrates the high efficiency of the assumed strain approach.

4.11. Shear wall with opening

In the last numerical example, a coupled shear wall is scrutinized to study the performance of the elements in the presence of opening. This structure, which is depicted in Figure 19, is made of elastic material with modulus of elasticity and Poisson's ratio equal to 2×10^7 and 0.2, respectively. The thickness of this structure is assumed 0.4. Lateral loads with intensity of $P = 500$ is applied to each story level of the left shear wall. The structure is analyzed by two meshes consisting of 48 and 192 quadrilateral elements (96 and 384 triangular elements). To achieve the near-exact solution, the coupled wall is analyzed by 26880 eight-node isoparametric elements (Q8). The obtained results for lateral displacements at different story levels are reported in Table 12.

It is evident that the suggested element provides the most accurate estimations. Based on the re-

Table 12. Lateral story displacements of the coupled shear wall.

	Element	Number of elements	Lateral displacement Story 2	Story 4	Story 6	Story 8
Quadrilateral elements	Q8	48 elements	0.56	1.53	2.59	3.64
		192 elements	0.68	1.82	3.02	4.16
	RY-R10-I	48 elements	0.77	2.07	3.40	4.71
		192 elements	0.78	2.07	3.44	4.71
	RY-R10-II	48 elements	0.69	1.88	3.13	4.28
		192 elements	0.74	2.00	3.32	4.65
	RY-Q14D	48 elements	0.90	2.62	4.61	6.63
		192 elements	1.14	3.22	5.49	7.70
	RY-Q18	48 elements	0.76	2.03	3.36	4.61
		192 elements	0.80	2.13	3.51	4.81
Triangular elements	RY-T10	48 elements	0.71	1.92	3.18	4.38
		192 elements	0.80	2.12	3.50	4.79
	RGR-T10	48 elements	0.76	2.03	3.29	4.54
		192 elements	0.85	2.26	3.63	4.96
	RGR-T10D	48 elements	0.73	1.94	3.19	4.45
		192 elements	0.82	2.14	3.55	4.86
	RGR-T11D	48 elements	**0.75**	**2.07**	**3.26**	**4.63**
		192 elements	**0.83**	**2.25**	**3.56**	**5.02**
Analytical solution		26880 elements	0.90	2.38	3.91	5.35

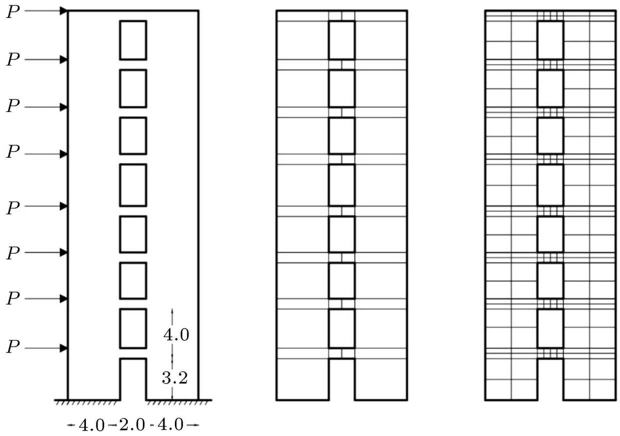

Figure 19. The coupled shear wall and the utilized meshes.

ported results for Q8 element, most of the strain-based membrane elements are more accurate and efficient. However, there is an exception about RY-Q14D, which becomes too flexible by using finer meshes and fails to converge to the exact response.

5. Conclusion

This study proposed a new triangular strain-based element with a second-order assumed strain field. Then, a series of well-known benchmark problems were solved using the proposed element and some of the other existing membrane elements and common displacement-based elements such as Q4, Q8, and LST. The obtained results clearly demonstrated the superiority of the strain-based formulation in accuracy and efficiency against displacement-based membrane elements. Various problems such as mesh sensitivity, shear, trapezoidal, and Poisson's locking were investigated, and the attained results showed that almost all of the plane elements formulated by the assumed strain approach were free from these shortcomings and could even compute response practical problems using coarse mesh of elements. Therefore, the strain-based elements completely fit with the definition of robust finite elements. It must be added that the newly proposed triangular plane element is among the best performing elements in all of the analyzed benchmark problems. This shows the merit of using higher-order assumed strain fields and imposing equilibrium equation on the opted strain components. The mentioned advantages make the assumed strain formulation an interesting alternative for developing robust finite elements of different types.

References

1. Zienkiewicz, O.C. and Taylor, R.L., *The Finite Element Method for Solid and Structural Mechanics*, Elsevier (2005).
2. Hughes, T.J.R., Taylor, R.L., and Kanoknukulchai, W. "A simple and efficient finite element for plate bending", *Int. J. Numer. Meth. Eng.*, **11**(10), pp. 1529-1543 (1977).
3. Reddy, J.N., *An Introduction to the Finite Element Method*, New York, USA: McGraw-Hill (1993).
4. Rezaiee-Pajand, M. and Gharaei-Moghaddam, N. "Analysis of 3D Timoshenko frames having geometrical and material nonlinearities", *Int. J. of Mech. Sci.*, **94**, pp. 140-155 (2015).
5. Rezaiee-Pajand, M. and Gharaei-Moghaddam, N. "Frame nonlinear analysis by force method", *Int. J. Ste. Str.*, **17**(2), pp. 609-629 (2017).
6. Rezaiee-Pajand, M. and Gharaei-Moghaddam, N. "Using co-rotational method for cracked frame analysis", *Meccanica*, **53**(8), pp. 2121-2143 (2018).
7. Rezaiee-Pajand, M. and Gharaei-Moghaddam, N. "Force-based curved beam elements with open radial edge cracks", *Mech. Adv. Mater. Struc.*, pp. 1-13 (2018). DOI: 10.1080/15376494.2018.1472326
8. Rezaiee-Pajand, M. and Gharaei-Moghaddam, N. "Vibration and static analysis of cracked and non-cracked non-prismatic frames by force formulation", *Eng. Str.*, **185**, pp. 106-121 (2019).
9. Sabir, A.B. "A rectangular and triangular plane elasticity element with drilling degrees of freedom", *2nd Int. Conf. on Var. Meth. in Engrg.*, Southampton, UK, pp. 17-25 (1985).
10. Sabir, A.B. and Sfendji, A. "Triangular and rectangular plane elasticity finite elements", *Thin. Wall. Struct.*, **21**(3), pp. 225-232 (1995).
11. Tayeh, S.M., *New Strain-Based Triangular and Rectangular Finite Elements for Plane Elasticity Problems*, The Islamic University of Gaza (2003).
12. Belarbi, M.T. and Bourezane, M. "On improved Sabir triangular element with drilling rotation", *Rev. Europ. Gén. Civ.*, **9**(9-10), pp. 1151-1175 (2005).
13. Belarbi, M.T. and Bourezane, M. "An assumed strain based on triangular element with drilling rotation", *Cour. Sav.*, **6**, pp. 117-123 (2005).
14. Belarbi, M.T. and Maalem, T. "On improved rectangular finite element for plane linear elasticity analysis", *Rev. Europ. Elém.*, **14**(8), pp. 985-997 (2005).
15. Rezaiee-Pajand, M. and Yaghoobi, M. "Formulating an effective generalized four-sided element", *Eur. J. Mech. A-Solid*, **36**, pp. 141-155 (2012).
16. Rezaiee Pajand, M. and Yaghoobi, M. "A free of parasitic shear strain formulation for plane element", *Res. Civ. Env. Eng.*, **1**, pp. 1-24 (2013).
17. Rebiai, C. and Belounar, L. "A new strain based rectangular finite element with drilling rotation for linear and nonlinear analysis", *Arch. Civ. Mech. Eng.*, **13**(1), pp. 72-81 (2013).
18. Rezaiee-Pajand, M. and Yaghoobi, M. "A robust triangular membrane element", *Lat. Amer. J. Sol. Struc.*, **11**(14), pp. 2648-2671 (2014).

19. Rezaiee-Pajand, M. and Yaghoobi M. "An efficient formulation for linear and geometric non-linear membrane elements", *Lat. Amer. J. Sol. and Struc.*, **11**(6), pp. 1012-1035 (2014).

20. Rebiai, C. and Belounar, L. "An effective quadrilateral membrane finite element based on the strain approach", *Measurement*, **50**, pp. 263-269 (2014).

21. Rebiai, C., Saidani, N., and Bahloul, E. "A new finite element based on the strain approach for linear and dynamic analysis", *Res. J. Appl. Sci. Eng. Tech.*, **11**(6), pp. 639-644 (2015).

22. Rezaiee-Pajand, M. and Yaghoobi, M. "Two new quadrilateral elements based on strain states", *Civ. Eng. Inf. J.*, **48**(1), pp. 133-156 (2015).

23. Hamadi, D., Ayoub, A., and Maalem, T. "A new strain-based finite element for plane elasticity problems", *Eng. Comp.*, **33**(2), pp. 562-579 (2016).

24. Rezaiee-Pajand, M. and Yaghoobi, M. "Geometrical nonlinear analysis by plane quadrilateral element", *Sci. Ira.*, **25**(5), pp. 2488-2500 (2018).

25. Rebiai, C. "Finite element analysis of 2-D structures by new strain based triangular element", *J. Mech.*, **35**(3) pp. 1-9 (2018).

26. Rezaiee Pajand, M., Gharaei Moghaddam, N., and Ramezani, M.R. "Two triangular membrane elements based on strain", *Int. J. Appl. Mech.*, **11**(1), p. 1950010 (2019).

27. Belounar, L. and Guenfoud, M. "A new rectangular finite element based on the strain approach for plate bending", *Thin Wall. Struct.*, **43**(1), pp. 47-63 (2005).

28. Hamadi, D., Abderrahmani, S., Maalem, T., and Temami, O. "Efficiency of the strain based approach formulation for plate bending analysis", *Int. J. Mech. Aero. Ind. Mechatr. Manufac. Eng.*, **8**(8), pp. 1408-1412 (2014).

29. Abderrahmani, S., Maalem, T., and Hamadi, D. "On improved thin plate bending rectangular finite element based on the strain approach", *Int. J. Eng. Res. Afr.*, **27**, pp. 76-86 (2016).

30. Abderrahmani, S., Maalem, T., Zatar, A., and Hamadi, D. "A new strain based sector finite element for plate bending problems", *Int. J. Eng. Res. Afr.*, **31**, pp. 1-13 (2017).

31. Belarbi, M.T. and Charif, A. "Novel sector element based on strain with in-plane rotations", *Rev. Europ. Elém.*, **7**(4), pp. 439-458 (1998) (In French).

32. Belounar, A., Benmebarek, S., and Belounar, L. "Strain based triangular finite element for plate bending analysis", *Mech. Adv. Mater. Struc.*, pp. 1-13 (2018). DOI: 10.1080/15376494.2018.1488310

33. Ashwell, D.G. and Sabir, A.B. "A new cylindrical shell finite element based on simple independent strain functions", *Int. J. Mech. Sci.*, **14**(3), pp. 171-183 (1972).

34. Djoudi, M.S. and Bahai, H. "Strain based finite element for the vibration of cylindrical panels with openings", *Thin wall. Struct.*, **42**(4), pp. 575-588 (1972).

35. Hamadi, D., Temami, O., Zatar, A., and Abderrahmani, S. "A comparative study between displacement and strain based formulated finite elements applied to the analysis of thin shell structures", *Int. J. Civ. Env. Struc. Const. Arch. Eng.,* **8**(8), pp. 875-880 (2014).

36. Mousa, A. and Djoudi, M. "New strain based triangular finite element for the vibration of circular cylindrical shell with oblique ends", *Int. J. Civ. Env. Eng.*, **15**(5), pp. 6-11 (2015).

37. Rezaiee-Pajand, M. and Yaghoobi, M. "An efficient flat shell element", *Meccanica*, **53**(4-5), pp. 1015-1035 (2018).

38. To, C.W.S. and Liu, M.L. "Hybrid strain based three-node flat triangular shell elements", *Finite Elem. Anal. Des.*, **17**(3), pp. 169-203 (1994).

39. Rezaiee-Pajand, M. and Yaghoobi, M. "A hybrid stress plane element with strain field", *Civ. Eng. Inf. J.,* **50**(2), pp. 255-275 (2017).

40. Belounar, L. and Guerraiche, K. "A new strain based brick element for plate bending", *Alex. Eng. J.*, **53**(1), pp. 95-105 (2014).

41. Guerraiche, K., Belounar, L., and Bouzidi, L. "A new eight nodes brick finite element based on the strain approach", *J. Solid Mech.*, **10**(1), pp. 186-199 (2018).

42. Messai, A., Belounar, L., and Merzouki, T. "Static and free vibration of plates with a strain based brick element", *Eur. J. Comp. Mech.*, pp. 1-21 (2018). DOI: 10.1080/17797179.2018.1560845

43. Alvin, K., Horacio, M., Haugen, B., and Felippa, C.A. "Membrane triangles with corner drilling freedoms-I. The EFF element", *Finite Elem. Anal. Des.*, **12**(3-4), pp. 163-187 (1992).

44. Allman, D.J. "A quadrilateral finite element including vertex rotations for plane elasticity analysis", *Int. J. Numer. Meth. Eng.*, **26**(3), pp. 717-730 (1988).

45. Cook, R.D. "A plane hybrid element with rotational DOF and adjustable stiffness", *Int. J. Numer. Meth. Eng.*, **24**(8), pp. 1499-1508 (1987).

46. MacNeal, R.H. and Harder, R.L. "A refined four-noded membrane element with rotational degrees of freedom", *Comput. Struct.*, **28**(1), pp. 75-84 (1988).

47. Cook, R.D. "Some options for plane triangular elements with rotational degrees of freedom", *Finite Eleme. Anal. Des.*, **6**(3), pp. 245-249 (1990).

48. Cook, R.D. "Modified formulations for nine-dof plane triangles that include vertex rotations", *Int. J. Numer. Meth. Eng.*, **31**(5), pp. 825-835 (1991).

49. Felippa, C.A. "A study of optimal membrane triangles with drilling freedoms", *Comput. Meth. Appl. M.*, **192**(16-18), pp. 2125-2168 (2003).

50. Timoshenko, S.P. and Goodier, J.N., *Theory of Elasticity*, 3rd Edn., McGraw-Hill: New York, U.S. (1934).

Biographies

Mohammad Rezaiee-Pajand received his PhD in Structural Engineering from University of Pittsburgh, Pittsburgh, PA, USA. He is currently a Professor at Ferdowsi University of Mashhad (FUM), Mashhad, Iran. His research interests are nonlinear analysis, finite element method, structural optimization, and numerical techniques.

Nima Gharaei-Moghaddam is currently a PhD candidate of Structural Engineering at Ferdowsi University of Mashhad (FUM). His research interests include numerical approaches for linear and nonlinear analysis of structures, applicable fracture mechanics, and composite structures.

Mohammad Reza Ramezani is an MSc student of Structural Engineering at Ferdowsi University of Mashhad, Iran, 2019. His research interests include generating optimal finite elements, enhancing strain based method and inelastic analysis of structures, and applying efficient elements in practical problems such as bearing-systems.